The Interaction of Ethylene with Perfect and Defective Ag(001) Surfaces

ARTICLE *in* THE JOURNAL OF PHYSICAL CHEMISTRY B · SEPTEMBER 2002

Impact Factor: 3.3 · DOI: 10.1021/jp025823k

The Interaction of Ethylene with Perfect and Defective Ag(001) Surfaces

Anton Kokalj,† Andrea Dal Corso,* Stefano de Gironcoli, and Stefano Baroni

SISSA - Scuola Internazionale Superiore di Studi Avanzati, I-34014 Trieste, Italy
INFM DEMOCRITOS National Simulation Center, I-34014 Trieste, Italy

Received: March 28, 2002; In Final Form: July 19, 2002

The adsorption of ethylene on perfect and defective Ag(001) surfaces has been studied and characterized using density functional theory. We find that ethylene binds rather weakly to the perfect surface and that the molecular geometry is correspondingly almost unchanged upon adsorption. The binding energy increases considerably near steps and adatoms, and this is correlated with a stronger hybridization between the silver d and ethylene π^* states.

1. Introduction

The epoxidation of ethylene (C_2H_4), catalyzed by silver, is one of the most important selective oxidation processes based on heterogeneous metallic catalysis. This reaction produces ethylene epoxide (oxirane), which is an important intermediate in the fabrication of glycols and polyols.[1] Much experimental work has been done and is still being done in order to understand the mechanisms of this reaction.[2−5] Some of the open questions are the location of stable adsorption sites of the molecule on Ag surfaces[6−16] and the role of surface defects in the adsorption process.[17]

Lattice imperfections are always present on surfaces. This is particularly the case of industrial catalysts which consist of small dispersed particles with a large variety and concentration of defects.[18] The importance of surface imperfections in the activation of catalysis was recognized already in the late 1920s by Taylor[19] and by Schwab and Pietsch.[20] Nowadays a large amount of experimental evidence indicates that the binding of adsorbates at surfaces is strengthened by the presence of defects.[21−24] In some cases the reactivity of the steps is so much larger than that of the terraces as to dominate the overall reaction rate at concentrations as low as 1% of step atoms.[25] Hammer and Nørskov[26] have recently reviewed the role of steps and defects in the adsorption and catalysis on transition metal surfaces. According to these authors, the enhanced binding energy of NO, O_2, N_2, and C_2H_4 and the lower barriers for adsorbate bond breaking would be determined by the smaller width of the d bands and by the higher energy of their center, both due to the reduced atomic coordination occurring at defects.

In addition to its specific importance, the adsorption of C_2H_4 on transition and noble metal surfaces can be considered as the prototype of adsorption of unsaturated hydrocarbons on metal catalysts. This process has received great attention from both experimentalists,[6−16,27−39] and theorists.[34,35,40−46] Chemisorption of ethylene on transition metals is known to proceed along two different states, characterized as π- and di-σ bonded.[31−34,42] In the π-bonded state the molecule is usually adsorbed on a *top* site,[42] and the sp^2 hybridization occurring in the gas phase is assumed to remain nearly intact upon adsorption. The di-σ bonding, which usually occurs on the *bridge* site,[42] is instead characterized by a substantial sp^3 rehybridization of the atomic orbitals of carbon. The bonding of C_2H_4 to the metal surface in the π-bonded state is usually described in terms of charge donation from the molecular π orbitals to d orbitals of the metal and of back-donation from the metal d orbitals to π^* orbitals.[34,44,47]

According to the thermal desorption spectroscopy (TDS) studies of Arvanitis et al.,[8] C_2H_4 desorbs from Ag(001) at a temperature of 143 K in the (sub)monolayer regime, while multilayers would desorb at 85 K. Subsequent investigations by Vattuone et al.[15,16] led these authors to characterize the desorption peak at 143 K as due to a π-bonded chemisorbed species, separated by an energy barrier from a physisorbed state having a desorption temperature lower than 105 K. In addition to these two states, Vattuone et al. also found evidence for the existence of a third, more strongly bound, chemisorbed state, which they characterize as di-σ bonded. Despite the importance of this system, the adsorption sites and geometries of ethylene on Ag(001) are still poorly characterized experimentally. Such a characterization was attempted by Tang et al.[11] who compared the near edge X-ray absorption spectra calculated by the multiple-scattering cluster method with experimental data.[8] These authors concluded that ethylene adsorbs onto the 4-fold hollow site with the C−C bond parallel to the surface. The C−C bond length and the Ag−C distance were found to be 1.40 and 1.96 Å, respectively.

While the C_2H_4 adsorption on transition metal surfaces has been the subject of several theoretical works, studies of adsorption of C_2H_4 on Ag surfaces are rather scarce. Carter et al.[40] studied olefin epoxidation using a cluster model with the generalized valence bond method. According to these authors, the interaction between C_2H_4 and a neutral Ag_3 cluster is repulsive, whereas ethylene was predicted to bind to an electrophilic Ag_3^+ cluster, with a binding energy of 0.33 eV. Avdeev et al.[46] performed calculations of the adsorption of ethylene on an oxidized Ag(111) surface (i.e., oxygen in the octahedral subsurface sites), using a cluster model with density functional theory (DFT): they predict that ethylene forms a π-complex on an oxidized surface with a binding energy of 0.62 eV and a carbon−silver distance of 2.9 Å. van den Hoek et al.[3] examined the role of subsurface oxygen in the ethylene epoxidation on the Ag(110) surface applying the $X\alpha$ method.

In this paper we report on the investigation of ethylene adsorption on perfect and defective Ag(001) surfaces, performed using DFT. We find that surface defects strongly affect the adsorption process, due to the enhanced hybridization between

* Corresponding author: Phone: +39-040-3787-428, Fax: +39-040-3787-528. E-mail: dalcorso@sissa.it
† Present address: Jožef Stefan Institute, 1000 Ljubljana, Slovenia.

10.1021/jp025823k CCC: $22.00
Published on Web 08/31/2002

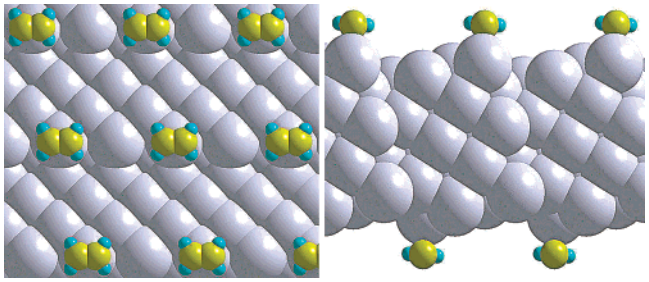

Figure 1. Ag(410) surface as a model of the monatomic step defect. Ethylene is adsorbed on the top of step Ag atom in (2 × 1) surface unit cell geometry. Top view is shown in the left panel, whereas a side view along the unit cell edge is shown in the right panel.

silver d_{π^*} (for the definition of the d_{π^*} orbital see note 48) and ethylene π^* states, thus increasing the chemisorption energy near them.

This paper is organized as follows. In section 2 we present the theoretical and computational frameworks of our work, along with a few relevant technical details. Section 3 contains our results: in section 3.1 we deal with the isolated constituents (Ag bulk and (001) clean surface, and C_2H_4 molecule in the gas phase); in section 3.2 we deal with C_2H_4 adsorption on Ag(001); in section 3.3 we address specifically the effects of surface defects on the adsorption process. In section 4 we discuss our results in terms of the electronic structure of the various systems studied in this work. Section 5 finally contains our conclusions.

2. Computational Method

Our calculations are based on DFT using the generalized gradient approximation (GGA) with the Perdew−Burke−Ernzerhof (PBE) energy functional.[49,50] We have used the pseudopotential method with ultrasoft pseudopotentials[51] and plane-wave basis sets up to a kinetic energy cutoff of 27 Ry (216 Ry for the charge-density cutoff). Brillouin-zone integrations have been performed with the special-point technique,[52] whereas the Fermi-surface effects have been treated by the smearing technique of Methfessel and Paxton,[53] using a smearing parameter of 0.03 Ry.

Perfect surfaces have been modeled using periodically repeated slabs of five Ag(001) layers, and molecular adsorption has been described with (2 × 2) and (3 × 3) surface supercells corresponding to coverages $\theta = 0.25$ monolayer (ML) and $\theta = 0.11$ ML, respectively. Brillouin-zone integrations were performed with a 4 × 4 and 3 × 3 Monkhorst−Pack[52] mesh for the (2 × 2) and (3 × 3) surface geometries, respectively. We have considered two types of defects: (i) monatomic steps and (ii) adatoms. Monatomic steps were modeled by the Ag(410) surface (see Figure 1). From the crystallographic point of view, the step model consists of 20 Ag(410) layers. This corresponds to terraces formed by five Ag(001) layers, merged together to form the Ag(410) surface. C_2H_4 was supposed to be adsorbed in a (2 × 1) geometry on *top* of step atoms with its C−C axis parallel to the direction of the step (see Figure 1). Adatoms were modeled with a (2 × 2) surface cell geometry and one silver adatom sitting on each side of a five-layer slab in a four-fold hollow site (see Figure 2). C_2H_4 was supposed to be adsorbed on *top* of silver adatoms. This model will be designated as Ag/Ag(001). Brillouin-zone integrations were performed with a 3 × 3 and a 4 × 4 Monkhorst−Pack mesh for C_2H_4/Ag(410) and C_2H_4/Ag/Ag(001), respectively.

To maintain the inversion symmetry of the unit cell, C_2H_4 molecules were placed symmetrically on both surfaces of the slabs. The thickness of the vacuum region (i.e., the distance between facing ethylene admolecules) was set to about 8 Å. We used the calculated bulk lattice parameter as the in-plane lattice spacing, and all the other structural parameters have been fully relaxed so as to minimize the total energy of the system.

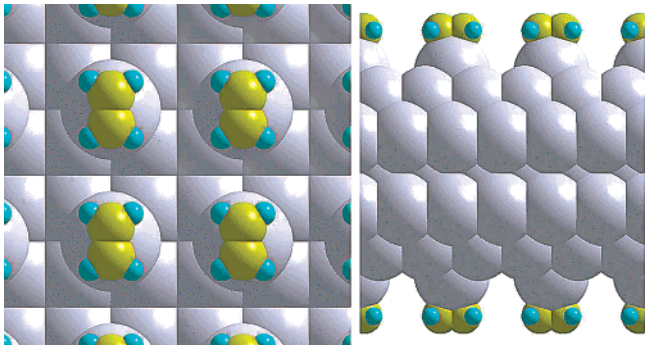

Figure 2. Model of adatom defect: the Ag adatom is sitting in a four-fold hollow site of a (2 × 2) surface geometry. A view from the top is shown in the left panel, whereas a side view is shown in the right panel.

The molecular binding energy (E_b) was calculated as

$$E_b = \frac{1}{2} \times [(E_{Sub} + 2 \times E_{Eth}) - E_{Eth/Sub}] \qquad (1)$$

where E_{Sub}, E_{Eth}, and $E_{Eth/Sub}$ are the total energies of the clean substrate, of the isolated ethylene molecule, and of the ethylene-on-substrate system, respectively. With this definition, stable adsorbates have positive binding energies.

When dealing with infinite (or, more generally, very large) systems, individual molecular orbitals and energy eigenvalues are not well suited for a thorough analysis of the results. The density of states (DOS) and some of its variants may be more convenient in this case. In the present study we have utilized the local DOS (LDOS), defined as

$$n(\epsilon, \mathbf{r}) = \sum_{v} \sum_{\mathbf{k}} |\psi_{v,\mathbf{k}}(\mathbf{r})|^2 \times \delta(\epsilon - \epsilon_{v,\mathbf{k}}) \qquad (2)$$

where $\psi_{v,\mathbf{k}}(r)$ is the vth occupied Bloch orbital at wave-vector $\mathbf{k}$, and $\epsilon_{v,\mathbf{k}}$ is the corresponding energy eigenvalue. The DOS projected onto individual atomic or molecular orbitals (PDOS), say $\phi(\mathbf{r})$, is defined as:[54]

$$n_\phi(\epsilon) = \sum_{v} \sum_{\mathbf{k}} |\langle \psi_{v,\mathbf{k}} | \phi \rangle|^2 \times \delta(\epsilon - \epsilon_{v,\mathbf{k}}) \qquad (3)$$

The bonding properties of molecular orbitals belonging to some given energy range, $[E_{min}, E_{max}]$, can be analyzed using the integrated local density of states (ILDOS), defined as

$$N(E_{min}, E_{max}, \mathbf{r}) = \int_{E_{min}}^{E_{max}} n(\epsilon, \mathbf{r})\, d\epsilon \equiv \sum_{v} \sum_{\mathbf{k}} \int_{E_{min}}^{E_{max}} |\psi_{v,\mathbf{k}}(\mathbf{r})|^2 \times \delta(\epsilon - \epsilon_{v,\mathbf{k}})\, d\epsilon \qquad (4)$$

In our case, due to the use of ultrasoft pseudopotentials, eqs 2, 3, and 4 contain also an augmentation term, and the corresponding expressions are written in note 55.

The charge transfer between the adsorbate and the substrate—as well as the formation of a chemical bond between them—can be characterized also in terms of the charge density difference, $\Delta n(\mathbf{r})$, defined as

$$\Delta n(\mathbf{r}) = n_{Eth/Sub}(\mathbf{r}) - [n_{Sub}(\mathbf{r}) + n_{Eth}(\mathbf{r})] \qquad (5)$$

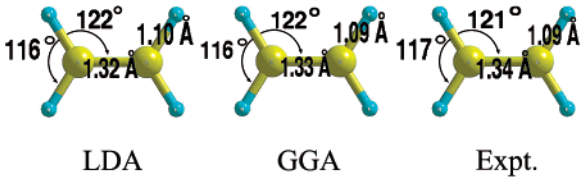

Figure 3. Comparison between the structural parameters of the ethylene molecule in the gas phase as calculated within LDA and GGA with the experimental geometry.[58]

where $n_{Eth/Sub}(\mathbf{r})$, $n_{Sub}(\mathbf{r})$, and $n_{Eth}(\mathbf{r})$ are the electron charge density distributions of the ethylene-on-substrate, clean substrate, and ethylene, respectively.

The calculations in this work have been performed using the PWSCF package,[56] while the molecular graphics have been done with the XCRYSDEN package.[57]

3. Results

3.1. Isolated Constituents: Ag Bulk, Ag(001) Clean Surface, and the C_2H_4 Molecule in the Gas Phase. The experimental lattice parameter of silver bulk is 4.09 Å,[58] whereas our GGA calculations yield 4.16 Å—an overestimation of 1.8%. Our results agree with previous studies performed by the full-potential linearized augmented-plane-wave method[59,60] (4.16/4.17 Å according to the GGA energy functional used), or by the linear-combination-of-atomic-orbitals method[60] (4.14 Å).

The properties of the clean Ag(001) surface have been calculated using 5-, 7-, and 9-layer slabs with a p(1 × 1) surface geometry. Here Brillouin-zone integrations were performed with a 12 × 12 Monkhorst−Pack mesh. The surface energy, σ, was estimated using the relation $\sigma = 1/2 \times \{E_{slab}(N) - N/2 \times [E_{slab}(N+2) - E_{slab}(N)]\}$, where N stands for the number of layers. The work function, ϕ, was calculated as the difference between the average electrostatic potential in the vacuum and the Fermi level. Our GGA calculations yield $\sigma = 0.05$ eV/Å^2 and $\phi = 4.2$ eV, while the corresponding experimental values are 0.08 eV/Å^2 (ref 61) and 4.6 eV (ref 58). The relaxations of the first and second layers were calculated to be $\Delta d_{12} = -1.8\%$ and $\Delta d_{23} = 0.3\%$. For more detailed analysis of the clean Ag(001) surface, see our study in ref 62.

The calculated and experimental structural parameters of ethylene in the gas phase are shown in Figure 3, whereas the valence molecular orbitals (MO) and their eigenvalues are displayed in Figure 4. The highest occupied molecular orbital (HOMO) and the lowest unoccupied molecular orbital (LUMO) are the bonding and antibonding combination of $2p_z$ orbitals of the two C atoms and are designated as π_{CC} and π^*_{CC}, respectively. The calculated HOMO(π_{CC})-LUMO(π^*_{CC}) gap is 5.7 eV.

3.2. Adsorption of Ethylene on Ag(001). Several possible configurations of ethylene on Ag(001) were examined in order to determine the relative stability of different adsorption sites (see Figure 5). For these calculations we used Ag(001) slabs consisting of just three layers. A comparison with a few test calculations made with five- or seven-layer slabs showed that three layers are sufficient to yield the correct relative stability of different adsorption sites. Molecular adsorption was modeled by a (2 × 2) surface unit cell, corresponding to an ethylene coverage of 0.25 ML. For the sake of comparison, we have also calculated the adsorption energies using the LDA.[63]

Our results are shown in Table 1. LDA and GGA predict different results both indicating, however, that adsorption on the *top* site is energetically favored. LDA predicts binding energies ranging from 0.25 to 0.55 eV and Ag−C distances in the range of 2.4−3.0 Å, whereas GGA predicts almost no ethylene-surface interaction, with binding energies ranging from 0.01 to 0.08 eV and Ag−C distances in the range of 2.9−4.2 Å.

Many previous studies indicate that LDA may over-bind molecules on metal surfaces.[26] To better assess how much can

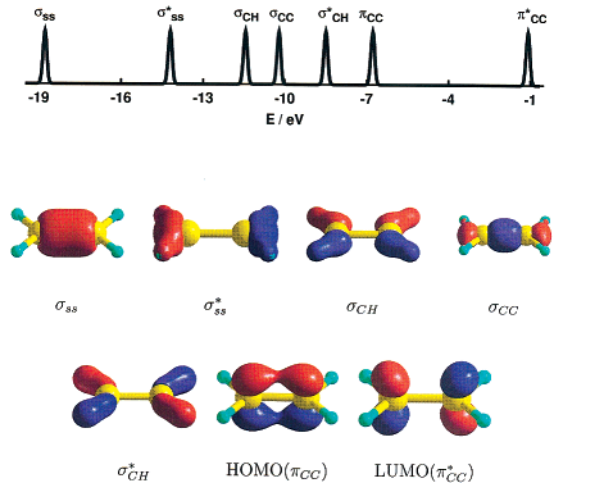

Figure 4. Plot of the valence molecular orbitals of gaseous C_2H_4, as calculated with the GGA. Their eigenvalues are shown at the top of the figure. States are labeled according to Demuth.[31]

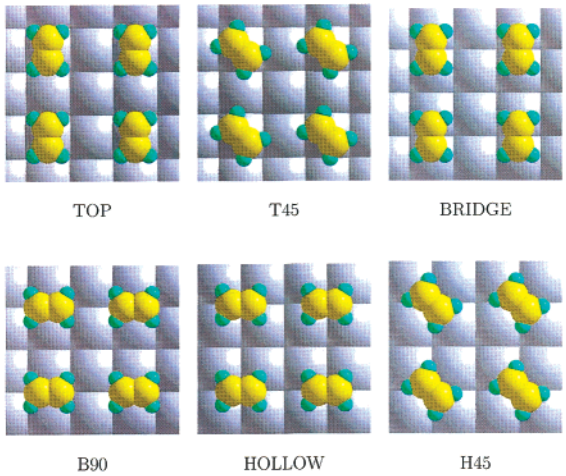

Figure 5. Different sites of ethylene on the perfect Ag(001) surface. The labels T45, B90 and H45 stand for "top rotated by 45°," "bridge rotated by 90°" and "hollow rotated by 45°", respectively.

TABLE 1: Calculated Binding Energies (E_b) and Structural Parameters of Ethylene Adsorbed on Various Sites of Ag(001) Surface[a]

method	site	E_b (eV)	d_{Ag-C} (Å)	d_{C-C} (Å)	h(Å)	τ_{HCCH}(°)
GGA						
	top	0.08	2.89	1.34	2.81	178
	T45	0.07	2.90	1.34	2.82	178
	bridge	0.04	3.52	1.33	3.42	180
	B90	0.03	4.21	1.33	3.89	180
	hollow	0.03	4.03	1.33	3.66	180
	H45	0.01	3.75	1.33	3.47	180
LDA						
	top	0.55	2.42	1.36	2.32	173
	bridge	0.42	2.49	1.35	2.38	171
	B90	0.34	3.02	1.34	2.59	180
	hollow	0.33	2.90	1.34	2.41	176
	H45	0.25	2.93	1.34	2.60	178

[a] The labels d_{Ag-C}, d_{C-C}, h and τ_{HCCH} stands for the Ag−C distance, C−C distance, height of ethylene molecule above the surface and the trans H−C=C−H dihedral angle, respectively.

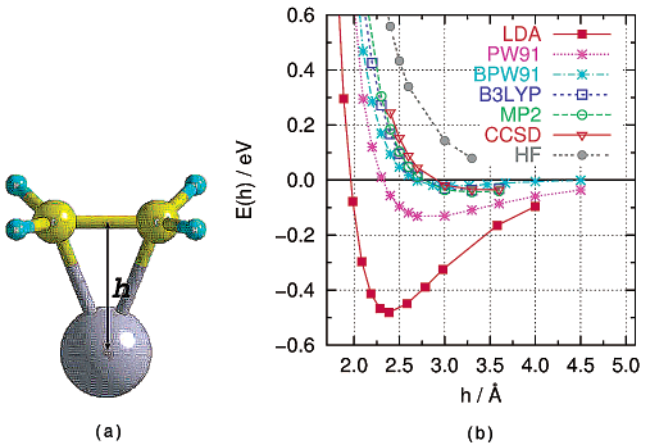

Figure 6. Interaction potentials of the $Ag(C_2H_4)$ complex calculated by different methods. The stepwise calculations were performed by constraining the height (h) of ethylene molecule and optimizing all the other structural parameters. For the explanation of labels, see text.

current DFT implementations be trusted in the present case, we have calculated the interaction between C_2H_4 and a single Ag atom using DFT with different energy functionals, and several quantum-chemical post Hartree−Fock methods.

3.2.1. The Ag(C_2H_4) Model Cluster. The interaction between ethylene and a single silver atom (see Figure 6) was calculated with the GAUSSIAN program,[64] which uses linear combinations of Gaussian-type orbitals as basis functions. The silver atom was described by the so-called LANL2DZ relativistic effective-core potential of Hay and Wadt, together with its associated basis set.[65−67] This basis set describes 19 valence electrons and consists of 8 s-, 6 p-, and 4 d-type functions, which were contracted to 3 s-, 3 p-, and 2 d-type functions. This can be written as (8s6p4d/3s3p2d). Carbon and hydrogen atoms were described in an all-electron scheme with basis sets[68] expressed in terms of (10s5p/3s2p) and (4s/2s), respectively. All these basis sets are of double-ζ valence quality.

Calculations were performed using the following different schemes: (i) DFT-LDA, with the Perdew−Zunger parameterization of the correlation energy;[63] (ii) DFT-GGA using the exchange-correlation functionals of Perdew−Wang[69] (labeled as PW91); (iii) DFT-GGA using the exchange functional of Becke[70] and correlation functional of Perdew−Wang (labeled as BPW91); (iv) DFT-GGA using Becke's three parameter hybrid exchange functional[71] and the Lee−Yang−Parr correlation functional[72] (B3LYP); (v) Hartree−Fock approximation (HF);[73] (vi) second-order Møller−Plesset perturbation theory[74] (MP2); (vii) coupled cluster method using single and double substitutions from the Hartree−Fock determinant[75] (CCSD). The potential interaction curves were obtained with series of stepwise minimization calculations, where the height (h) of ethylene above the Ag atom was kept fixed, but all the other structural parameters were allowed to relax to the (constrained) energy minimum.

The results of these calculations are shown in Figure 6. These results indicate that GGA substantially improves upon LDA. We chose therefore to adopt a GGA description of the exchange and correlation effects for the rest of the paper, in the favor of the PBE functional, consistently with other previous studies of ours on adsorption on transition metal surfaces.[62,76−80]

3.3. Comparison between Perfect and Defective Surfaces. In this section we address the effects of surface defects on the adsorption of C_2H_4 on Ag(001). We saw in section 3.2 that both the LDA and GGA predict the *top* adsorption site to be energetically favored. Even though the relevant energy differences predicted by the GGA are of the order of our estimated overall theoretical accuracy (a few 10 meV), for the sake of definiteness we choose to concentrate on this most stable site throughout the rest of the paper. Our calculations were done using slabs of five Ag layers. Steps and adatom defects were modeled with the Ag(410) and Ag/Ag(001) structures described in section 2. In Table 2 we report the binding energies and structural parameters of ethylene adsorbed on the perfect Ag(001) surface, the monatomic Ag(410) step, and on top of an adatom defect.

TABLE 2: GGA Calculated Binding Energies (E_b) and Structural Parameters for Ethylene Top Adsorption on Perfect and Defective Ag(001) Surfaces (monatomic step and adatom defects)[a]

adsorption system	E_b(eV)	d_{Ag-C} (Å)	d_{C-C} (Å)	h(Å)	τ_{HCCH}(°)
(2×2)-C_2H_4/Ag(001)	0.084	2.91	1.34	2.83	178
(3×3)-C_2H_4/Ag(001)	0.119	2.66	1.35	2.57	177
(2×1)-C_2H_4/Ag(410)	0.248	2.53	1.35	2.45	176
(2×2)-C_2H_4/Ag/Ag(001)	0.317	2.47	1.36	2.34	174

[a] These data refer to five-layer slab calculations. The monatomic step defect was modeled by the Ag(410) surface, whereas Ag/Ag(001) indicates the adatom defect. The labels have the same meaning as in Table 1.

Let us first discuss the case of the perfect surface. The binding energy is very small: depending on the coverage, it ranges from 0.08 for 0.25 ML to 0.12 eV for 0.11 ML. The adsorbate/substrate height ranges between 2.6 and 2.8 Å (the corresponding Ag−C distances are 2.7 and 2.9 Å, respectively) and the molecular geometry is almost unchanged upon adsorption. These heights are substantially larger than those estimated by Tang et al. from a fit of multiple-scattering-cluster results to experimental NEXAFS spectra (1.96 ± 0.03 Å).[11] Also, the results of these authors seem to indicate that the favored adsorption site should be the four-fold hollow. Our calculations are consistent with the results of other GGA studies which predict larger ethylene/surface distances for surfaces such as Pd and Pt[43−45] whose lattice parameters are smaller than that of silver, and where the ethylene is known to be more strongly bound.[43−45] Furthermore, our calculated distances compare well to the value of 2.9 Å obtained by Avdeev et al. for the ethylene adsorption on the oxidized Ag(111) surface,[46] using cluster DFT/B3LYP calculations.

The slightly larger binding energy calculated for (3×3)-C_2H_4/Ag(001) (0.12 eV) than for (2×2)-C_2H_4/Ag(001) (0.08 eV) suggests that a repulsive lateral ethylene−ethylene interaction may be induced by charge transfer from ethylene to the substrate. This conclusion is supported by the drop of the work function upon adsorption ($\Delta\phi = -0.7$ eV for (2×2)-C_2H_4/Ag(001)) and by inspection of the charge density difference resulting upon adsorption, which is displayed in the top panel of Figure 7. We conclude that, in contrast with more reactive transition metal surfaces (see refs 43−45 or our previous work on benzene on Pd(110)[77]), the Ag(001) surface is not able to form a strong chemical bond with the ethylene molecule. This result does not explain the experimental findings of Vattuone et al.[15,16] who observed two chemisorbed states: a π-bonded state stable up to $T \sim 140$ K (corresponding to an estimated binding energy ~ 0.35 eV), and an even more stable di-σ state.

The failure of our calculations to account for the above experimental data, indicates that other effects, not accounted for in our modeling of the adsorption geometry, may be responsible for a stabilization of the chemical bond between C_2H_4 and Ag surfaces. In order to try to reconcile the predictions of DFT-GGA with experiments, we now discuss the adsorption

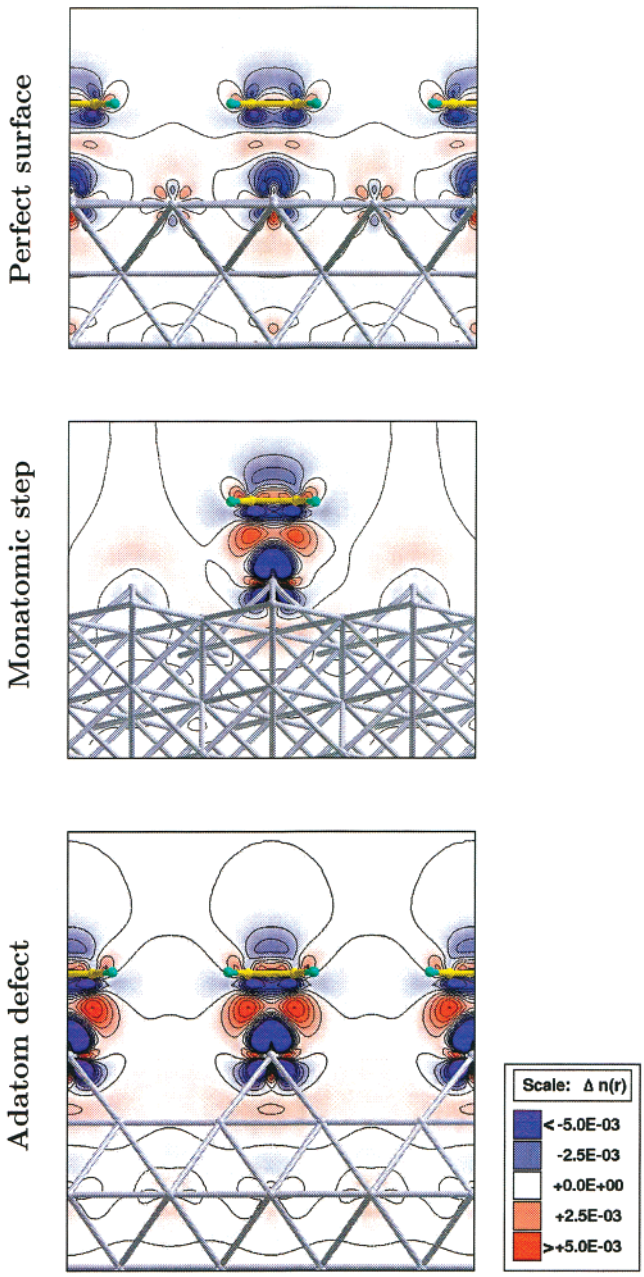

Figure 7. Charge difference density (i.e., $\Delta n(\mathbf{r}) = n_{\mathrm{Eth/Sub}}(\mathbf{r}) - [n_{\mathrm{Sub}}(\mathbf{r}) + n_{\mathrm{Eth}}(\mathbf{r})]$). From top to bottom: $\Delta n(\mathbf{r})$ of (2 × 2)-C_2H_4/Ag(001), (2 × 1)-C_2H_4/Ag(410), and (2 × 2)-C_2H_4/Ag/Ag(001) adsorption systems. Contours are drawn in linear scale from −0.005 to 0.005 e/a_0^3, with the increment of 0.001 e/a_0^3. The blue color represents the electron deficit regions, while the electron excess regions are colored in red (i.e., charge flows from blue to red regions).

of ethylene on defective sites of Ag(001). For atomic steps, we chose as a model the Ag(410) surface described in section 2. Adsorption on an isolated adatom defect, which represents the defective site of lowest possible coordination, was modeled by the (2 × 2)-Ag/Ag(001) structure also described in section 2, where one ethylene is supposed to be adsorbed on every adatom. Even though the resulting concentration of defects (0.25 ML) is unrealistically large, we believe that this model, which is computationally affordable, is adequate for understanding the role of a lower coordination in the adsorption phenomena. A lower surface concentration of adatoms would decrease the lateral intermolecular interaction and reduce the adatom-induced effects of the substrate, but we do not expect that this would substantially modify the conclusions reported below.

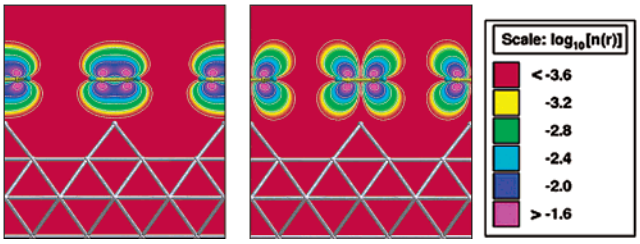

Figure 8. The HOMO(π) (left panel) and LUMO(π^*) (right panel) states of ethylene layer superimposed on the (2 × 2)-Ag/Ag(001) substrate. Contours are drawn in a logarithmic scale (5 contours from 2.5E−4 to 2.5E−2 e/a_0^3) and plots are colored rainbow-like (the magnitude of the plotted orbitals increases from red to blue).

The binding of ethylene is sensibly enhanced on the defective sites with respect to the perfect surface. The binding energy at the step edge is 0.25 eV, and it is even larger on top of an adatom (0.32 eV). The corresponding height of the adsorbate above the substrate is 2.45 and 2.34 Å for the step and adatom sites, respectively. It is worth noticing that E_b correlates with the adsorbate height (h) above the substrate, carbon−carbon distance (d_{CC}), and trans HCCH dihedral angle (τ_{HCCH}). Stronger bonding is connected with a smaller height of the molecule above the substrate. The carbon−carbon distance also undergoes a small elongation of 0.02 Å when going from the perfect surface to the adatom site. This is an indication of a tiny back-donation from the d orbitals to the antibonding π^* orbital of ethylene. Finally, the adsorbed ethylene molecule is almost planar, and its deviation from the planar geometry is larger for the more reactive defective sites.

The experimental TDS peak temperature of ethylene is ∼140 K which, assuming the desorption to be nonactivated and the adsorption to be first order,[81] would lead to an estimated heat of adsorption of 0.35 eV. Our results for adsorption on defective sites are in better agreement with experiments and suggest that the relatively large binding energy of C_2H_4 on Ag(001) may possibly be due to the presence of surface defects on the substrate. Recently Vattuone et al.[17,82] performed experiments on Ag(410) and observed nearly unitary sticking probability at the step edge and stable adsorption in the π-bonded state with the TDS peak temperature of ∼140 K. This provides strong support to our conclusions on the enhancing role of defects on molecular adsorption.

4. Discussion

To understand the mechanisms which determine the enhancement of molecular adsorption at surface defects, we examine now in some detail the electronic structures of the various systems studied in this work.

In Figure 7 we display the charge density difference, i.e., the difference between the density of the adsorption system and its constituents (molecule and substrate). This figure distinctly demonstrates the increased accumulation of the charge in the region between the ethylene and the substrate (red regions located below the carbon atoms) for the monatomic step and the adatom defect, which is an indication of the enhanced chemical bonding. To help the interpretation of Figure 7, we plotted the ethylene HOMO(π) and LUMO(π^*) orbitals superimposed on the (2 × 2)-Ag/Ag(001) structure in Figure 8. Notably, a comparison of these two figures reveals the similarity between the region of the accumulated charge (red regions below the carbon atoms) shown in Figure 7 and the ethylene LUMO(π^*) state pictured in Figure 8. Indeed, these plots suggest that the coupling of the ethylene π^* state with the silver d_{π^*} (see

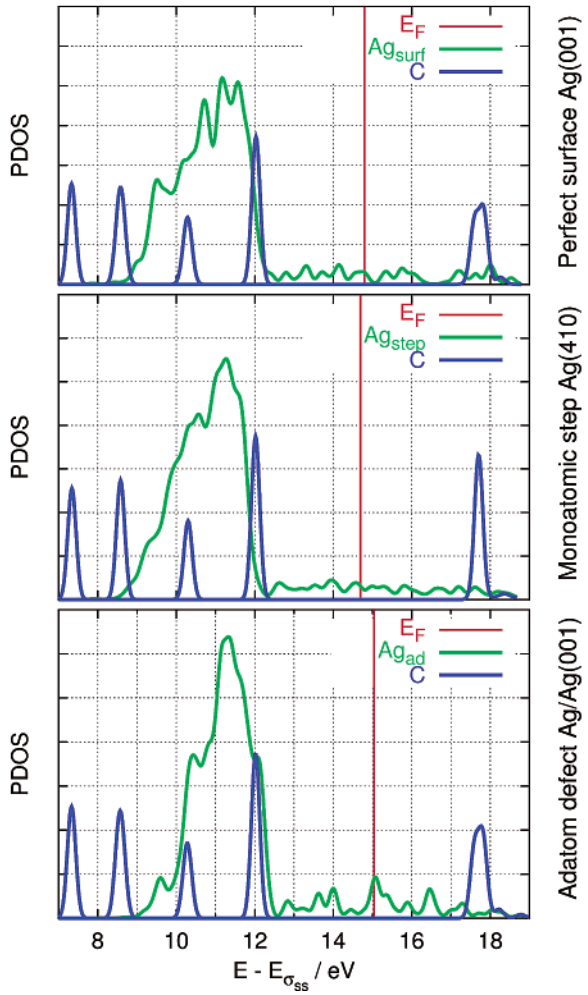

Figure 9. Density of states of the isolated subsystems (surface or molecule, see note 83), projected onto the carbon atom of the ethylene molecule and onto the surface silver atoms (PDOS). In the case of defective surfaces, the DOS is projected onto defect atoms. From top to bottom panels: (2×2)-C_2H_4/Ag(001), (2×1)-C_2H_4/Ag(410), and (2×2)-C_2H_4/Ag/Ag(001). The ethylene σ_{ss} level is chosen as the zero energy level for these plots. The LUMO peak is broader in the top and bottom panel due to the smaller lateral ethylene−ethylene distance.

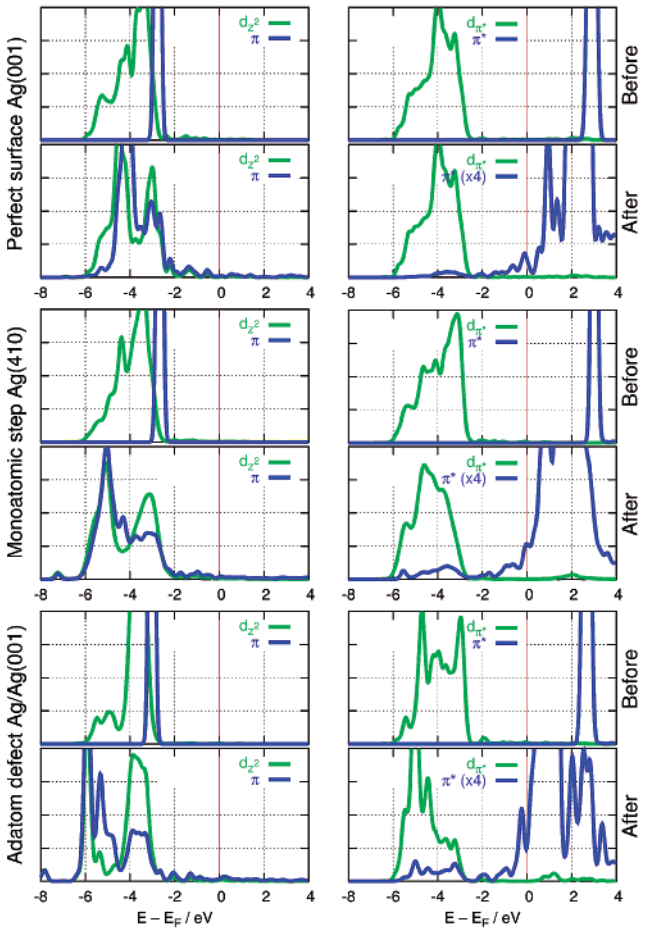

Figure 10. DOS projected onto the ethylene π and π^* orbitals and silver d_{z^2} and d_{π^*} states. From top to bottom: the PDOS of (2×2)-C_2H_4/Ag(001), (2×1)-C_2H_4/Ag(410), and (2×2)-C_2H_4/Ag/Ag(001). On the left we show the projection onto π and d_{z^2}, while on the right we show the PDOS of π^* and d_{π^*} states. Note that in order to make some relevant features visible (see text) we have magnified four-times ($\times 4$) the π^* PDOS of the equilibrium systems. For each system (perfect surface, monatomic step, and adatom defect), the top panels show the PDOS of the isolated subsystems (see note 83), while the bottom panels refer to the equilibrium ethylene/substrate distance.

note 48) states only takes place for the monatomic step and adatom defective sites.

To further analyze the electronic structure and the bonding between the ethylene and the substrate, we start by considering the densities of states projected onto the orbitals of selected atoms of the two isolated subsystems (molecule and surface, see note 83), which are displayed in Figure 9. The molecular levels are clearly identified as peaks in the DOS. In these plots the ethylene σ_{ss} level is chosen as the zero of the energy. The C_2H_4 HOMO is located at the top of the surface silver d bands, which is about 3 eV below the Fermi level, whereas the LUMO is about 3 eV above the Fermi level. The d bands of the adatom are much narrower than those of the atoms on the perfect surface—as a consequence of a lower coordination—whereas the width of the d bands at a monatomic step is intermediate between the two.

In Figure 10 we compare the PDOS projected onto selected atomic and molecular orbitals (ethylene π and π^*, and silver d_{z^2} and d_{π^*}) when the interaction between the molecule and the surface is taken into account or neglected, i.e., the molecule is at the equilibrium distance or far from the surface, respectively. Although ethylene binds very weakly to the surface and its equilibrium distance is quite large, the left panels of the figure demonstrate that the molecular π state is broadened substantially as a consequence of its hybridization with silver d_{z^2} states, which are also strongly affected by the interaction. Both the C_2H_4 π and Ag d_{z^2} contributions to the DOS display a rather well defined doublet structure where the bonding and antibonding components are split (more pronouncedly so in the adatom case). Both components are well below the Fermi level, resulting in a weak net contribution to the binding energy.

The interplay between bonding and antibonding states in the adsorption of C_2H_4 onto Ag(001) is further illustrated in Figure 11, where we display the ILDOS (see section 2) for (2×2)-C_2H_4/Ag(001), as calculated for two energy windows ([−6.0, − 3.5] eV and [−3.0, 0.0] eV), corresponding to the two peaks of the DOS of this system, projected onto Ag-d_{z^2} and C_2H_4-π orbitals (see Figure 10). The states in the first energy range are bonding states between ethylene π orbital and the silver d_{z^2} orbital as shown by the charge visible in the region between the molecule and the substrate. The states in the second energy window, which are in the range of the second peak in the DOS of Figure 10, have antibonding character as shown by the depletion of charge visible in the same region. The fact that both bonding and antibonding states are below the Fermi energy results in a weak overall bond between C_2H_4 and the clean Ag-

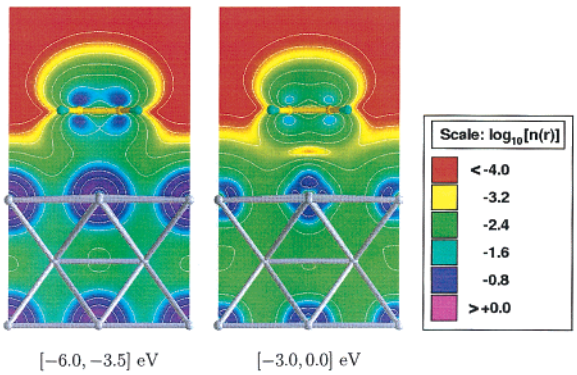

Figure 11. Integrated local density of states (ILDOS) of (2 × 2)-C_2H_4/Ag(001). Left panel: ILDOS in the energy window [−6.0, −3.5] eV. Right panel: the energy window is shifted to [−3.0, 0.0] eV. The Fermi energy is taken as the zero energy level. Contours are drawn in a logarithmic scale (nine contours from 1.0 to 10^{-4} e/a_0^3) and plots are colored rainbow-like (the magnitude of the plotted ILDOS increases from red to blue).

(001). The occupation of the ethylene π state upon adsorption, is estimated to be about 1.94 e, 1.90 e, and 1.90 e for the perfect surface, monatomic step, and adatom defect, respectively. A larger bonding−antibonding splitting in the step and adatom cases seems to shift a tiny percentage of π states above the Fermi level. However, these numbers should be taken with care, since in the projections of the plane-wave eigenstates to the atomic or molecular orbitals, typically 1−2% of charge is missing. Nevertheless, we can conclude that the bonding and antibonding interactions cancel each other to a large extent, and hence these interactions should not give a net stabilizing effect.

The right side of Figure 10 displays the ethylene π^* and silver d_{π^*} contributions to the total DOS. As far as the interaction between C_2H_4 and the substrate is concerned, the relevant trends can be related to the adsorption-induced variations of the π^* and d_{π^*} PDOS below the Fermi energy. For the perfect surface, the d_{π^*} PDOS is practically unaffected by adsorption, and the π^* PDOS, while modified by adsorption, does not contribute to the binding because it vanishes below the Fermi energy both before and after adsorption. Moving to the monatomic step, we notice that adsorption both shifts the d_{π^*} PDOS toward lower energies[84] and pushes a tiny fraction of π^* electrons (magnified four-times in the Figure for better visibility) below the Fermi level.[85] Both effects determine an enhancement of the binding. Passing finally to the adatom defect, these two effects are even stronger, leading us to the conclusions that the strength of this interaction increases when lowering the coordination of the metal atoms that bind the molecules due to an increased interaction between the π^* and d_{π^*} orbitals. This trend is also consistent with the observation that the greater the binding energy the larger the carbon−carbon distance of ethylene, due to the filling of the π^* orbital, which destabilizes the carbon−carbon bond and increases the bond length.

5. Conclusions

In this paper we have addressed the adsorption of C_2H_4 on Ag(001) surfaces and found it to be weak in the absence of surface defects. We also found that surface defects substantially enhanced the molecular binding onto the surface, possibly providing a mechanism for the relatively high desorption temperatures observed experimentally (about 140 K) and for the large sticking probability recently reported for C_2H_4 on Ag(410). Work is in progress to extend the present research to the important case where ethylene and oxygen are coadsorbed on Ag(001).

Acknowledgment. The authors would like to thank to David Loffreda, Mario Rocca, Giacinto Scoles, and Luca Vattuone for helpful discussions. This work has been supported by INFM ("Iniziativa trasversale calcolo parallelo" and Sezioni F and G) and by the Italian MIUR (PRIN). All numerical calculations were performed on the Cray-T3E and IBM-SP3 computers at CINECA in Bologna (Italy).

References and Notes

(1) van Santen, R. A. Epoxidation Catalysis Using Heterogeneous Catalysts. In *Handbook of Heterogeneous Catalysis*, Vol. 5; Ertl, G., Knözinger, H., Weitkamp, J., Eds.; Wiley-VCH: Weinheim, 1997; Chapter 4, pp 2244−2252.
(2) Campbell, C. T.; Paffet, M. T. *Surf. Sci.* **1984**, *139*, 396.
(3) van den Hoek, P. J.; Baerends, E. J.; van Santen, R. A. *J. Phys. Chem.* **1989**, *93*, 6469.
(4) Bukhtiyarov, V. I.; Boronin, A. I.; Savchenko, V. I. *J. Catal.* **1994**, *150*, 262.
(5) Bukhtiyarov, V. I.; Boronin, A. I.; Prosvirin, I. P.; Savchenko, V. I. *J. Catal.* **1994**, 268.
(6) Backx, C.; de Groot C. P. M. *Surf. Sci.* **1981**, *115*, 382.
(7) Krüger, B.; Benndorf, C. *Surf. Sci.* **1986**, *178*, 704.
(8) Arvanitis, D.; Baberschke, K.; Wenzel, L.; Döber, U. *Phys. Rev. Lett.* **1986**, *57*, 3175.
(9) Solomon, J. L.; Madix, J.; Stöhr, J. *J. Chem. Phys.* **1990**, *93*, 8379.
(10) Slater, D. A.; Hollins, P.; Chesters, M. *Surf. Sci.* **1994**, *306*, 155.
(11) Tang, J. C.; Shen, J. F.; Chen, Y. B. *Surf. Sci. Lett.* **1991**, *224*, L125.
(12) Zhou, X.-L.; White, J. M. *J. Phys. Chem.* **1992**, *96*, 7703.
(13) Akita, M.; Hiramoto, S.; Osaka, N.; Itoh, K. *J. Phys. Chem. B* **1999**, *103*, 10189.
(14) Akita, M.; Osaka, N.; Hiramoto, S.; Itoh, K. *Surf. Sci.* **1999**, *427−428*, 374.
(15) Vattuone, L.; Valbusa, U.; Rocca, M. *Phys. Rev. Lett.* **1999**, *82*, 4878.
(16) Vattuone, L.; Savio, L.; Valbusa, U.; Rocca, M. *Chem. Phys. Lett.* **2000**, *331*, 177.
(17) Rocca, M.; Savio, L.; Vattuone, L. *Surf. Sci.* **2002**, *502-503*, 331.
(18) Somorjai, G. A. *Introduction to surface chemistry and catalysis*; John Willey & Sons: New York, 1994.
(19) Taylor, H. S. *J. Phys. Chem.* **1926**, *30*, 145.
(20) Schwab, G. M.; Pietsch, E. *Z. Phys. Chem. B* **1928**, *1*, 385.
(21) Somorjai, G. A. *Chemistry in Two Dimensions: Surfaces*; Cornell University Press: Ithaca and London, 1981.
(22) Ramsier, R. D.; Gao, Q.; Waltenburg, N. H.; Yates, J. T., Jr. *J. Chem. Phys.* **1994**, *100*, 6837.
(23) Zambelli, T.; Wintterlin, J.; Trost, J.; Ertl, G. *Science* **1996**, *273*, 1688.
(24) Savio, L.; Vattuone, L.; Rocca, M. *Phys. Rev. Lett.* **2001**, *87*, 276101.
(25) Dahl, S.; Logadottir, A.; Egeberg, R. C.; Larsen, J. H.; Chorkendorff, I.; Törnqvist, E.; Nørskov, J. K. *Phys. Rev. Lett.* **1999**, *83*, 1814.
(26) Hammer, B.; Nørskov, J. K. *Adv. Catal.* **2000**, *45*, 71.
(27) Ertl, G. *Surf. Sci.* **1967**, *7*, 309.
(28) Yu, K. Y.; Spicer, W. E.; Lindau, I.; Pianetta, P.; Lin, S. *Surf. Sci.* **1976**, *57*, 157.
(29) Fischer, T. E.; Kelemen, S. R. *Surf. Sci.* **1977**, *69*, 485.
(30) Demuth, J. E. *Surf. Sci.* **1978**, *76*, L603.
(31) Demuth, J. E. *IBM J. Res. Dev.* **1978**, *22*, 265.
(32) Demuth, J. E. *Surf. Sci.* **1979**, *84*, 315.
(33) Cassuto, A.; Mane, M.; Hugenschmidt, M.; Dolle, P.; Jupille, J. *Surf. Sci.* **1990**, *237*, 63.
(34) Weinelt, M.; Huber, W.; Zebisch, P.; Steinrück, H.-P.; Pabst, M.; Rösch, N. *Surf. Sci.* **1992**, *271*, 539.
(35) Weinelt, M.; Huber, W.; Zebisch, P.; Steinrück, H.-P.; Reichert, B.; Birkenheuer, U.; Rösch, N. *Phys. Rev. B* **1992**, *46*, 1675.
(36) Turton, S.; Jones, R. G. *Surf. Sci.* **1997**, *377−379*, 719.
(37) Linke, R.; Becker, C.; Pelster, T.; Tanemura, M.; Wandelt, K. *Surf. Sci.* **1997**, *377−379*, 655.
(38) Okuyama, H.; Ichihara, S.; Ogasawara, H.; Kato, H.; Komeda, T.; Kawai, M.; Yoshinobu, J. *J. Chem. Phys.* **2000**, *112*, 5948.
(39) Okuyama, H.; Kato, H.; Kawai, M.; Yoshinobu, J. *J. Chem. Phys.* **2000**, *113*, 2866.
(40) Carter, E. A.; Goddard, W. A., III *Surf. Sci.* **1989**, *209*, 243.
(41) Triguero, L.; Pettersson, L. G. M.; Minaev, B.; Ågren, H. *J. Chem. Phys.* **1998**, *108*, 1193.

(42) Bocquet, M.-L.; Sautet, P. *Surf. Sci.* **1998**, *415*, 148.
(43) Ge, Q.; King, D. A. *J. Chem. Phys.* **1999**, *110*, 4699.
(44) Pallassana, V.; Neurock, M. *J. Catal.* **2000**, *191*, 301.
(45) Watwe, R. M.; Cortright, R. D.; Mavrikakis, M.; Nørskov, J. K.; Dumesic, J. A. *J. Chem. Phys.* **2001**, *114*, 4663.
(46) Avdeev, V. I.; Zhidomirov, G. M. *Surf. Sci.* **2001**, *492*, 137.
(47) March, N. H. *Chemical Bonds Outside Metal Surfaces;* Plenum Press: New York and London, 1986.
(48) We define the symbol d_{π^*}, which stands for the linear combination of atomic d orbitals having the same symmetry as the π^* orbital of the adsorbed molecule. According to the geometries presented in Figures 1, 2, and 5, d_{π^*} is d_{yz} for the perfect surface and adatom defect, while for the monatomic step the appropriate orbital is $d_{\pi^*} = d_{xz}$.
(49) Perdew, J. P.; Burke, K.; Ernzerhof, M. *Phys. Rev. Lett.* **1996**, *77*, 3865.
(50) For the sake of comparison, we have also made a few test calculations using the local density approximation (LDA) with the exchange correlation energy parametrized by Perdew and Zunger.[63]
(51) Vanderbilt, D. *Phys. Rev. B* **1990**, *41*, 7892.
(52) Monkhorst, H. J.; Pack, J. D. *Phys. Rev. B* **1976**, *13*, 5188.
(53) Methfessel, M.; Paxton, A. T. *Phys. Rev. B* **1989**, *40*, 3616.
(54) Projected densities of states (PDOS) are calculated using the orthonormalized atomic orbitals, say $\tilde{\phi}(\mathbf{r})$, which are defined as: $\tilde{\phi}_\mu(\mathbf{r}) = \sum_\nu S_{\mu\nu}^{-1/2}\phi_\nu(\mathbf{r})$, where $S_{\mu\nu}^{-1/2}$ is the element of the square root inverse of the overlap matrix $\mathbf{S}$ of the atomic orbitals $\phi_i(\mathbf{r})$, whose elements are: $S_{\mu\nu} = \langle\phi_\mu|\phi_\nu\rangle$. The charge associated with the atomic orbital μ is then $Q_\mu = \sum_\nu^{\mathrm{occ}}\sum_{\mathbf{k}}|\langle\psi_{\nu,\mathbf{k}}|\tilde{\phi}_\mu\rangle|^2$. This is the so-called Löwdin population analysis.
(55) In the case of ultrasoft pseudopotentials, eqs 2, 3, and 4 contain an additional term due to augmentation charges, hence the corresponding eq 2 is: $n(\epsilon, \mathbf{r}) = \sum_\nu\sum_{\mathbf{k}}\{|\psi_{\nu,\mathbf{k}}(\mathbf{r})|^2 + \sum_{I,nm}Q_{nm}^I(\mathbf{r})\langle\psi_{\nu,\mathbf{k}}|\beta_n^I\rangle\langle\beta_m^I|\psi_{\nu,\mathbf{k}}\rangle\} \times \delta(\epsilon - \epsilon_{\nu,\mathbf{k}})$. The corresponding eq 3 is $n_\phi(\epsilon) = \sum_\nu\sum_{\mathbf{k}}\langle|\psi_{\nu,\mathbf{k}}|S|\phi\rangle|^2 \times \delta(\epsilon - \epsilon_{\nu,\mathbf{k}})$, while the corresponding eq 4 is $N(E_{\min}, E_{\max}, \mathbf{r}) = \sum_\nu\sum_{\mathbf{k}}\int_{E_{\min}}^{E_{\max}}\{|\psi_{\nu,\mathbf{k}}(\mathbf{r})|^2 + \sum_{I,nm}Q_{nm}^I(\mathbf{r})\langle\psi_{\nu,\mathbf{k}}|\beta_n^I\rangle\langle\beta_m^I|\psi_{\nu,\mathbf{k}}\rangle\} \times \delta(\epsilon - \epsilon_{\nu,\mathbf{k}})\, d\epsilon$. The symbols used in these equations are the same as in ref 86.
(56) Baroni, S.; Dal Corso, A.; de Gironcoli, S.; Giannozzi, P. "PWSCF and PHONON: Plane-Wave Pseudo-Potential Codes", http://www.pwscf.org/, 2001.
(57) The address of the XCRYSDEN[87,88] WEB page is: http://www-k3.ijs.si/kokalj/xc/XCrySDen.html.
(58) Lide, D. R., Ed.; *CRC Handbook of Chemistry and Physics* 74th ed.; CRC Press: Boca Raton, Florida, 1993.
(59) Khein, A.; Singh, D. J.; Umrigar, C. J. *Phys. Rev. B* **1995**, *51*, 4105.
(60) Kokalj, A.; Causà, M.; Dovesi, R., unpublished data.
(61) Tyson, W. R.; Miller, W. A. *Surf. Sci.* **1972**, *62*, 267.
(62) Cipriani, G.; Loffreda, D.; Dal Corso, A.; de Gironcoli, S.; Baroni, S. *Surf. Sci.* **2002**, *501*, 182.
(63) Perdew, J. P.; Zunger, A. *Phys. Rev. B* **1981**, *23*, 5048.
(64) Frisch, M. J.; Trucks, G. W.; Schlegel, H. B.; Gill, P. M. W.; Johnson, B. G.; Robb, M. A.; Cheeseman, J. R.; Keith, T.; Petersson, G. A.; Montgomery, J. A.; Raghavachari, K.; Al-Laham, M. A.; Zakrzewski, V. G.; Ortiz, J. V.; Foresman, J. B.; Cioslowski, J.; Stefanov, B. B.; Nanayakkara, A.; Challacombe, M.; Peng, C. Y.; Ayala, P. Y.; Chen, W.; Wong, M. W.; Andres, J. L.; Replogle, E. S.; Gomperts, R.; Martin, R. L.; Fox, D. J.; Binkley, J. S.; Defrees, D. J.; Baker, J.; Stewart, J. P.; Head-Gordon, M.; Gonzalez, C.; Pople, J. A. *Gaussian 94*; Gaussian, Inc.: Pittsburgh, PA, 1995.
(65) Hay, J.; Wadt, W. R. *J. Chem. Phys.* **1985**, *82*, 270.
(66) Hay, J.; Wadt, W. R. *J. Chem. Phys.* **1985**, *82*, 284.
(67) Hay, J.; Wadt, W. R. *J. Chem. Phys.* **1985**, *82*, 299.
(68) Dunning, H., Jr.; Hay, P. J. In *Modern Theoretical Chemistry*; Schaefer, H. F., III, Ed.; Plenum: New York, 1976.
(69) Perdew, J. P.; Wang, Y. *Phys. Rev. B* **1992**, *45*, 13244.
(70) Becke, A. D. *Phys. Rev. A* **1988**, *38*, 3098.
(71) Becke, A. D. *J. Chem. Phys.* **1993**, *98*, 5648.
(72) Lee, C.; Yang, W.; Parr, R. G. *Phys. Rev. B* **1988**, *37*, 785.
(73) Roothaan, C. C. J. *Rev. Mod. Phys.* **1960**, *32*, 179.
(74) Møller, C.; Plesset, M. S. *Phys. Rev.* **1934**, *46*, 618.
(75) Cizek, J. *Adv. Chem. Phys.* **1969**, *14*, 35.
(76) Cipriani, G. *Ab Initio Study of Oxygen Adsorption on Selected Transition Metal Surfaces*, Thesis, International School for Advanced Studies, Trieste, Italy, 2000.
(77) Favot, F.; Dal Corso, A.; Baldereschi, A. *Europhys. Lett.* **2000**, *52*, 698.
(78) Kokalj, A.; Dal Corso, A.; de Gironcoli, S.; Baroni, S. *Surf. Sci.* **2002**, *507-510*, 62.
(79) Favot, F.; Dal Corso, A.; Baldereschi, A. *Phys. Rev. B* **2001**, *63*, 115416.
(80) Favot, F.; Dal Corso, A.; Baldereschi, A. *J. Chem. Phys.* **2001**, *114*, 483.
(81) Adamson, A. W. Chemisorption and Catalysis. In *Physical Chemistry of Surfaces*, 5th ed.; John Wiley & Sons: New York, 1990; Chapter 17, pp 690−692.
(82) Savio, L.; Vattuone, L.; Rocca, M. Understanding the Pressure Gap in Catalysis: Steps and Terraces in the Interaction of O_2 and C_2H_4 with Ag(410). In *20th European Conference on Surface Science*, *Europhysics conference abstract*, Vol. 25J.; Szymonski, M., Czuba, P., Krok, F., Eds.; European Physical Society: Krakow, Poland, 2001.
(83) The isolated subsystems were simulated with a supercell where a molecule was placed in the center of a vacuum region of about 12 Å separating two adjacent metallic slabs.
(84) The center of d_{π^*} PDOS, $\int_{-\infty}^{\epsilon_F}\epsilon n_{d\pi^*}(\epsilon)\, d\epsilon$, is shifted to lower energies upon adsorption: −0.07 eV, −0.42 eV, and −0.73 eV for the perfect surface, monatomic step, and adatom defect, respectively.
(85) The population of π^* states below the Fermi energy upon adsorption is 0.05 e, 0.10 e, and 0.15 e for the perfect surface, monatomic step, and adatom defect, respectively.
(86) Laasonen, K.; Pasquarello, A.; Car, R.; Lee, C.; Vanderbilt, D. *Phys. Rev. B* **1993**, *47*, 10142.
(87) Kokalj, A. *J. Mol. Graphics Modelling* **1999**, *17*, 176.
(88) Kokalj, A.; Causà, M. Scientific Visualization in Computational Quantum Chemistry. In *Proceedings of High Performance Graphics Systems and Applications European Workshop*; CINECA − Interuniversity Consortium: Bologna, Italy, 2000.